Extending MWA-Scale Ionospheric Calibration for SKA-Low

Daniel A. Mitchell

Abstract – We detail a new technique for measuring variable dispersive delays from irregularities and turbulence in the Earth's ionosphere. Such measurements are crucial for maximizing the imaging dynamic range of modern low-frequency interferometric arrays used in radio astronomy. Ionospheric delays vary with time, frequency, line of sight, and antenna location, all of which can lead to the decoherence of astronomical signals in complicated ways. A common approach to reducing these variations is to measure excess phase shifts between each antenna and one or more known radio source(s) and correct for these shifts when imaging or modeling the radio sky. This is a general approach that works well in a range of situations. However, the resolution of the corrections in line of sight and time can be limited by the large number of free parameters and the availability of calibrators with sufficient brightness.

A different approach, suitable for arrays that do not exceed the typical ionospheric irregularity scale of a few kilometers, is to measure an excess delay gradient across the array for each calibration direction. Such measurements contain less spatial information across the array but can be made using weaker sources or shorter time intervals. In effect, degrees of freedom across the array are traded for degrees of freedom across the sky. In this paper, we combined aspects of each approach. We measured excess delay between clusters of antennas along with low-order delay fluctuations within each cluster, where ionospheric shifts are expected to have a high level of correlation. We showed this approach was versatile over a range of signal-to-noise ratios and had particular benefits at lower signal levels.

1. Introduction

The variability of the Earth's ionosphere poses significant challenges for low-frequency radio interferometry. Dispersive ionospheric delays can be highly variable with time, frequency, line of sight, and antenna location, leading to variable refraction, decoherence, and depolarization in any or all of these dimensions. This impacts all areas of low-frequency radio astronomy; it will be a particular challenge for the Epoch of Reionization imaging, where foreground galactic and extragalactic emission needs to be accurately suppressed or avoided, and systematics—particularly those varying with frequency or angle—need to be understood with high precision.

Lonsdale [1] considers four observing regimes with distinct ionospheric calibration needs. In the first, both the array and the field of view are small relative to any ionospheric irregularities of concern. In contrast, in the second, the array is larger than the irregularities, and antennas may look through different ionospheric patches. In both cases, the field of view is small enough that any effect can be considered constant across an image and can be corrected using antenna-based delay calibration. In regime three, the field of view is larger, and ionospheric delays change with direction; however, the array is small enough that for a given direction, the delays are assumed to vary in a linear fashion across it. This results in apparent angular shifts of radio sources that increase with wavelength squared. The final calibration regime is the general case of a large array with a large field of view.

The low-frequency Square Kilometre Array (SKA-Low; [2]) falls in the final ionospheric calibration regime. One approach to calibrating such an array is to divide the field of view into several smaller calibration fields and measure antenna-based phase or delay errors for each (see [3] for an example at SKA-Low angular scales). Phase corrections can be applied directly in facet-based imaging but will often be used to generate spatial models for other imaging algorithms (e.g., [4]). This works well; however, the initial antenna-based measurements ignore the fact that delays will be correlated across short antenna separations. Such correlated information could increase the sensitivity and allow for more calibration directions. To extract more information, one can imagine constraining a comprehensive model using the interferometric measurements directly, with knowledge of the expected response of each antenna to perhaps thousands of radio sources across the field of view. However, this can become a large and complex problem. Complementing antenna-based delays with other intermediate calibration products can be a more tractable approach.

The Murchison Widefield Array (MWA; [5]) has the majority of its antennas within a few square kilometers, and when ionospheric conditions are benign, a regime three calibration strategy can be employed. The MWA Real-Time System (RTS) was developed with this in mind [6], but rather than measuring offsets in the image domain, delay gradients across the array are measured using the visibility data. While such gradients increase with the observing wavelength, this can be included in the calibration model, and all baseline and frequency data can be combined into a single bivariate solution per direction.

Manuscript received 22 December 2023.

Daniel Mitchell is with CSIRO Space & Astronomy, PO Box 76, Epping NSW 1710, Australia; e-mail: Daniel.Mitchell@csiro.au.

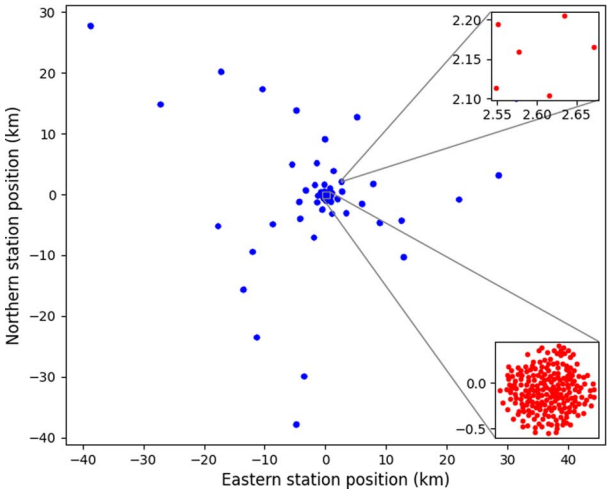

Figure 1. SKA-Low station layout *LOWBD2* from https://developer.skao.int/projects/ska-sdp-datamodels.

While this parameterization may probe ionospheric delays across the array with lower spatial resolution than antenna-based terms, the large increase in data points per model parameter means that fainter radio sources can be used as calibrators, increasing the sampling across the field of view. This approach may not seem suitable for geographically large arrays like SKA-Low; however, many of the SKA-Low antennas are grouped in the inner kilometer of the array, and the other antennas are grouped in clusters (see Figure 1). In this work, we demonstrate how the RTS approach can be extended to include higher-order variations for the inner array while simultaneously constraining additional low-order variations across the remaining antenna clusters.

2. Formulation

In the RTS, the effect of the ionosphere is parameterized as an angular shift that increases with wavelength λ squared as follows: $l = l_0 + \lambda^2 a_l$, $m = m_0 + \lambda^2 a_m$. (l_0, m_0) are the true direction cosine coordinates of a radio source, and (a_l, a_m) are the unknown fit parameters that, when multiplied by λ^2, give the ionospheric offset [6]. Ignoring wide-field w terms, this results in a visibility phase shift of $-2\pi\lambda^2(ua_l + va_m)$, and all of the baselines and frequencies can be combined in a single least squares fit for a_l and a_m. For higher-order parameterizations of delay with antenna location, relative *uv* terms are replaced with higher-order coordinate terms, but the same general approach can be used. The approach used in this work is as follows (Note: More details for the approach taken here are given at https://developer.skao.int/projects/ska-sdp-func-python).

Suppose that the antennas of an array are grouped into clusters. These can be arbitrary groups of antennas; however, it is assumed that they are near enough to one another that their ionospheric distortions have some degree of correlation. In the initial version of this work, the inherent clusters from the SKA Low configuration shown in Figure 1 were used. Suppose also that the excess phase shift at antenna location (x, y), relative to a cluster center (x_c, y_c), is decomposed into orthonormal basis functions, $Z_{c,0}(x - x_c, y - y_c)$, $Z_{c,1}(x - x_c, y - y_c)$, …, such that the phase shift for antenna j at frequency f can be written

$$\phi_{j,f} = -2\pi\lambda_f^2 \sum_p a_{c_j,p} Z_{c_j,p}(x_j - x_{c_j}, y_j - y_{c_j}). \quad (1)$$

We have added a subscript to the cluster index c_j to indicate that this is the cluster associated with antenna j. In the case of linear functions that return gradients in the *uv* plane, when array baselines are formed the problem is reduced to the *uv* coordinates and the RTS parameters. In this paper, we used Zernike polynomials, which include those linear gradients as first-order terms. Harmonic functions could also be added to model structured ionospheric disturbances.

We form *normal equations* for the parameters, $a_{c_j,p}$, specifying the amount of delay aligned with each basis function, and solve using the linear least squares method. As in the RTS, we use a first-order expansion of the complex phase exponential and fit for the excess delay in the imaginary part of weighted visibilities. Weighting by the complex conjugate of model visibilities removes expected phase shifts and scales by the optimal amount for calibration models with visibility amplitudes that vary across the *uv* plane. Fitting is an iterative process, and for many unknowns, it can be more efficient to split each iteration into the smaller normal equations for each cluster and solve them separately. This has been done for the results in this paper, but the full-equation results are equivalent.

A limited number of low-order basis functions were used to avoid over-fitting the data and help restrict the modeling process to ionospheric effects. The functions can be different for different clusters; for example, higher-order basis functions can be used for large central clusters in arrays like SKA-Low. The zeroth-order functions, $Z_{c,0}$, were used to fix the delay between clusters. A small number of large clusters requires higher-order terms to capture the delay variation across the array, while many smaller clusters are more dependent on the inter-cluster $Z_{c,0}$ terms. As the size of the clusters approaches one antenna, the algorithm approaches antenna-dependent delay calibration algorithms, such as in [7].

3. Results and Discussion

The algorithm has been worked into the ska-sdp-func-python package, one of the SKA python repositories with reference implementations of several array calibration and imaging tasks. Simulations were run for all 224 stations in the SKA-Low core (with a diameter of 1 km) and up to 66 stations from each of the three spiral arms for a maximum baseline of 28 km. The full layout is shown in Figure 1. In

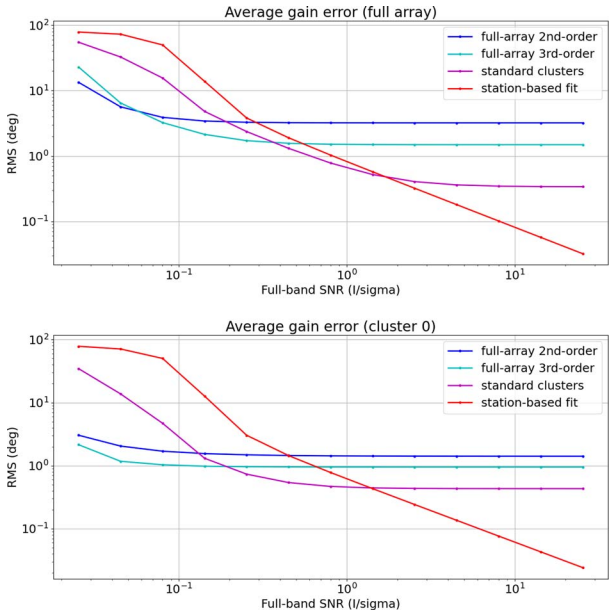

Figure 2. RMS of phase errors for all stations (top) and just the core stations (bottom) as a function of the calibrator signal-to-noise level averaged over several independent runs to smooth over noise. Errors are shown for a range of cluster types as follows: a single full-array cluster with second-order Zernike polynomial basis functions (in dark blue); the same but with third-order basis functions (in cyan); a large central cluster with third-order basis functions plus a small first-order cluster of each grouping of six remote stations (in magenta); and single-station clusters using only the intercluster $Z_{c,0}$ terms (in red).

the following discussion, any "antenna-based" effects refer to individual low stations. The solution interval was 10 seconds and 150 MHz, with frequencies running from 100 to 250 MHz. This is a nominal spectral window, chosen to be near the center of the SKA-Low band and with a likely bandwidth. Visibility noise was added using the system equivalent flux density spectrum from [8], and phase screens with Kolmogorov turbulence were generated with a diffractive scale of 10 km at 150 MHz, following the method described in [9]. These are quiet ionospheric conditions for radio astronomy, and restricting the maximum baseline length has helped to limit phase ambiguities. More work is needed to make the current implementation more robust to phase wrapping.

A simple point source was used as the calibrator, to keep the signal-to-noise calculation simple. However, the algorithm was set up with appropriate weighting for complex fields with multiple radio components and source morphology. The approach was also well suited to direction-dependent calibration algorithms like peeling [6]; the small number of free parameters helped to limit over-fitting and deep integrations across baselines and frequencies helped to reduce coupling between different lines of sight.

Figure 2 shows the root mean square (RMS) of station phase errors as a function of the calibrator signal-to-noise ratio (SNR). Errors were generated by subtracting the known input phase shifts from the fitted values and are shown for a few different cluster types as follows:

1. A single cluster containing all stations. At this extreme, the algorithm is like the RTS approach of [6], albeit with higher-order parameters. Results are shown for second- and third-order Zernike polynomial basis functions. These are shown in blue.
2. Each station is its own single-station "cluster," with delays modeled by the zeroth-order, intercluster $Z_{c,0}$ terms (1). At this extreme, the algorithm has reduced to antenna-based delay calibration. This is shown in red.
3. An intermediate setup with a central cluster comprising stations from the core and an additional cluster for each group of six remote stations (see Figure 1). Delays were modeled with third-order Zernike polynomials for the large inner cluster, but limited to first order for the smaller remote clusters. Shown in magenta.

The full-array cluster can only model delay variations on the largest scales, and increasing the signal level cannot recover details at finer scales, as seen by the RMS floor to the right of the plots. However, this moderate accuracy is maintained down to very low SNR. On the other hand, independent antenna-based delay solutions have no inner-scale restrictions, and the errors continue to decrease as the SNR increases. But there are fewer constraints per parameter and these fits are less capable at low SNR levels. As expected, using both higher orders and multiple clusters results in errors that sit between these two situations.

The lower panel of Figure 2 shows phase error RMS for just the inner core of stations. The antenna-based delay results are much the same as the full-array results, but the relative errors are small in this inner region when solving for clusters. This is the region of particular interest for the Epoch of Reionization science.

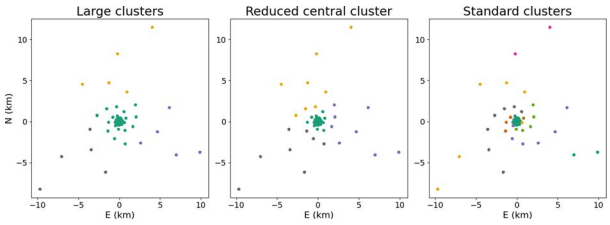

Figure 3. Three cluster types shown in Figure 4. On the left are four similar sized clusters, distinguished by point color (i.e., a central green cluster and three outer clusters). The central panel has a reduced size for the central dense green cluster and larger outer clusters. Only core stations are included in the inner green cluster on the right panel. Each of the other points in this panel expands into a group of six remote stations (as in Figure 1), with each six-station group forming its own cluster.

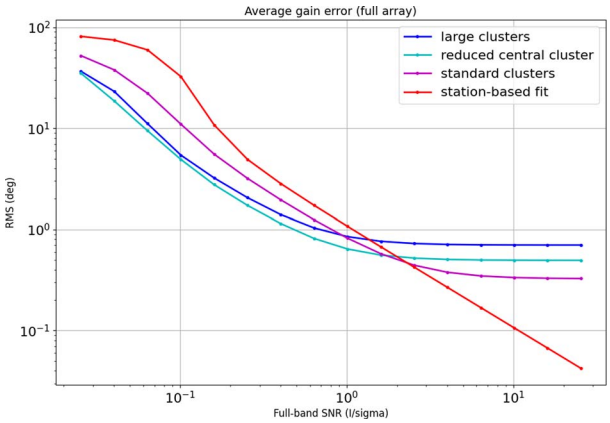

Figure 4. RMS of phase errors as a function of the calibrator signal-to-noise level, averaged over several independent runs to smooth over noise. Errors are shown for the three cluster groupings described in Figure 3: Four large clusters in dark blue, four clusters with a physically smaller inner cluster in cyan, and an inner cluster for core stations plus small clusters for groups of six remote stations in magenta. The results for single-station clusters are also shown in red.

We see similar effects when changing the size of clusters. Figure 4 shows the RMS error across stations for the three cluster groupings shown in Figure 3. As expected and evident in previous figures, larger clusters have more signal and work better at low signal levels, but they require larger basis functions with limited sensitivity to higher-order fluctuations that could be probed by stronger calibrators.

It should be noted that these results were for benign ionospheric conditions. When the ionosphere becomes active, and there is more power on smaller spatial scales, low-order basis functions across large clusters will not have the resolution to model it. In these situations, smaller clusters or antenna-based delay solutions may be required. Looking forward, the level of clustering and/or the order of the aperture functions could be selected based on the flux density of a calibration field and the ionospheric conditions. This could help with the deconvolution of moderate-strength radio sources but could also help to maximize the number of paths through the ionosphere and minimize the errors of subsequent global ionospheric models.

Finally, the algorithm described here also offers competitive computational performance, being similar in many ways to antenna-based solvers but with fewer parameters. However, a detailed performance analysis is beyond the scope of the current paper, and comparisons against similar solvers, such as those described in [3] and [7], are left for future work. Furthermore, the new algorithm should offer better isolation from other calibration directions and other confusing radio sources due to the large amount of averaging per model parameter. However, other packages can average in other ways, and detailed comparisons are needed to assess the overall differences.

4. Conclusion

Low-frequency arrays look through a complex and dynamic ionosphere, and how to go about correcting for associated signal delays can depend on the nature of the array. General techniques that work well for large arrays may ignore correlated information at the array level that would help to better calibrate the array, while techniques that work well for small arrays may not be applicable in general. In this paper, we have described an algorithm that can bridge the gap between these situations without requiring an expensive, comprehensive ionospheric model.

The algorithm has been shown to have advantages at a range of signal-to-noise levels, but in particular when the signal level is low and antenna-based algorithms break down. The flexibility of general-purpose, antenna-based algorithms is limited by having fewer data constraints per fit parameter—meaning less signal relative to the noise—as well as the risk of over-fitting the data. Both issues can limit the frequency with which delay solutions can be generated in time and line of sight. Algorithms that fit low-order delay functions across the array aperture can accumulate much more signal per fit parameter but are limited in how much spatial variation can be modeled with a reasonable number of parameters. The new algorithm seeks a middle ground. It splits the array into station clusters, with each cluster handled as in the antenna-based algorithms while allowing for a limited amount of delay variation across clusters.

5. Acknowledgments

The foundations of this work were carried out as part of a NEC4 Framework Contract with the SKA Observatory. The author is grateful to Danielle Fenech from the SKA Data Processing Agile Release Train Program Team as Feature Owner for feature SP-3328.

6. References

1. C. J. Lonsdale, “Configuration Considerations for Low Frequency Arrays,” From Clark Lake to the Long Wavelength Array: Bill Erickson's Radio Science ASP Conference Series, Santa Fe, New Mexico, September 8–11, 2004, p. 399.
2. P. E. Dewdney, P. J. Hall, R. T. Schilizzi, and T. J. L. W. Lazio, “The Square Kilometre Array,” *Proceedings of the IEEE*, **97**, 8, August 2009, pp. 1482-1496.
3. T. W. Shimwell, M. J. Hardcastle, C. Tasse, et al., “The LOFAR Two-Metre Sky Survey – V. Second Data Release,” *Astronomy and Astrophysics*, **659**, A1, February 2022.
4. H. T. Intema, S. van der Tol, W. D. Cotton, A. S. Cohen, I. M. van Bemmel, and H. J. A. Rottgering, “Ionospheric Calibration of Low Frequency Radio Interferometric Observations Using the Peeling Scheme I. Method Description and First Results,” *Astronomy and Astrophysics*, **501**, 3, May 2009.
5. S. J. Tingay, R. Goeke, J. D. Bowman, et al., “The Murchison Widefield Array: The Square Kilometre Array Precursor at Low Radio Frequencies,” *Publications of the Astronomical Society of Australia*, **30**, e007, January 2013.

6. D. A. Mitchell, L. J. Greenhill, R. B. Wayth, et al., "Real-Time Calibration of the Murchison Widefield Array," *IEEE Journal of Selected Topics in Signal Processing*, **2**, 5, August 2008.
7. M. J. Rioja, R. Dodson, and T. M. O. Franzen, "LEAP: An Innovative Direction-Dependent Ionospheric Calibration Scheme for Low-Frequency Arrays," *Monthly Notices of the Royal Astronomical Society*, **478**, 2, May 2018, pp. 2337-2349.
8. M. Sokolowski, S. J. Tingay, D. B. Davidson, et al., "What is the SKA-Low Ssensitivity for Your Favourite Radio Source," *Publications of the Astronomical Society of Australia*, **39**, e015, April 2022, p.e015.
9. R. G. Lane, A. Glindemann and J. C. Dainty, "Simulation of a Kolmogorov Phase Screen," *Waves in Random Media*, **2**, August 1991, pp. 209-224.